Article

TRANSPARENT PROCESS

EMBO reports

Molecular architecture of the yeast Elongator complex reveals an unexpected asymmetric subunit arrangement

Dheva T Setiaputra[1], Derrick TH Cheng[1], Shan Lu[2], Jesse M Hansen[1], Udit Dalwadi[1], Cindy HY Lam[1], Jeffrey L To[1], Meng-Qiu Dong[2] & Calvin K Yip[1,*]

Abstract

Elongator is a ~850 kDa protein complex involved in multiple processes from transcription to tRNA modification. Conserved from yeast to humans, Elongator is assembled from two copies of six unique subunits (Elp1 to Elp6). Despite the wealth of structural data on the individual subunits, the overall architecture and subunit organization of the full Elongator and the molecular mechanisms of how it exerts its multiple activities remain unclear. Using single-particle electron microscopy (EM), we revealed that yeast Elongator adopts a bilobal architecture and an unexpected asymmetric subunit arrangement resulting from the hexameric Elp456 subassembly anchored to one of the two Elp123 lobes that form the structural scaffold. By integrating the EM data with available subunit crystal structures and restraints generated from cross-linking coupled to mass spectrometry, we constructed a multiscale molecular model that showed the two Elp3, the main catalytic subunit, are located in two distinct environments. This work provides the first structural insights into Elongator and a framework to understand the molecular basis of its multifunctionality.

Keywords electron microscopy; Elongator; structure; tRNA modification
Subject Categories RNA Biology; Structural Biology
DOI 10.15252/embr.201642548 | Received 13 April 2016 | Revised 18 October 2016 | Accepted 25 October 2016 | Published online 21 November 2016
EMBO Reports (2017) 18: 280–291

See also: **MI Dauden *et al***

Introduction

The Elongator complex is an evolutionarily conserved multisubunit protein complex initially identified as a component of the elongating form of RNA polymerase II [1]. Subsequent studies revealed that Elongator participates in various processes, including histone acetylation [2], transcription regulation [3,4], α-tubulin acetylation [5], and tRNA modification [6]. In particular, Elongator plays an essential role in the addition of 5-methoxycarbonylmethyl and 5-carbamoylmethyl to the wobble base pair of transfer RNAs (tRNAs) that stabilizes codon–anticodon interactions and facilitates translation [7]. Because of its broad range of activities, deficiencies in human Elongator have been shown to give rise to serious pathological conditions such as familial dysautonomia and other neurological disorders [8–11].

Elongator consists of six unique subunits (Elp1, Elp2, Elp3, Elp4, Elp5, and Elp6), with two copies of each protein associating into a dodecameric ~850 kDa holo-complex [12,13]. Previous biochemical studies have shown that the Elongator subunits are organized into two subassemblies: one composed of Elp1, Elp2, and Elp3 (Elp123), and the other one composed of Elp4, Elp5, and Elp6 (Elp456) [12,14]. Elp123 houses Elp3, the main catalytic subunit, which contains both a Gcn5-related N-acetyltransferase histone acetyltransferase (HAT) domain and a radical S-adenosylmethionine (SAM) domain [15]. Elp456 forms a heterohexameric RecA-like ATPase ring, which possesses ATP-modulated tRNA binding activity [13]. How the multiple catalytic domains of Elongator are regulated is poorly understood.

Despite a fairly extensive understanding of the domain composition of Elongator and recent advances in delineating the structural properties of individual Elongator subunits (e.g., Elp1 C-terminal domain, Elp2, and Elp456) [13,16–18], the overall architecture and subunit organization of this complex remain unclear. We have isolated the holo-Elongator complex from yeast *Saccharomyces cerevisiae* and obtained the first structural data on this complex using an integrative approach combining single-particle electron microscopy (EM), cross-linking coupled to mass spectrometry (CXMS), and multiscale modeling. Our data revealed an unexpected asymmetric overall architecture and subunit organization of Elongator and provided a framework to understand the molecular basis of Elongator's multifunctionality.

Results

Yeast Elongator adopts an asymmetric overall architecture

We isolated the full Elongator complex from a *S. cerevisiae* strain encoding C-terminally FLAG-tagged Elp1 (Fig 1A). Densitometry

1 Department of Biochemistry and Molecular Biology, The University of British Columbia, Vancouver, BC, Canada
2 National Institute of Biological Sciences, Beijing, Beijing, China
*Corresponding author. Tel: +1 604 827 3976; E-mail: calvin.yip@ubc.ca

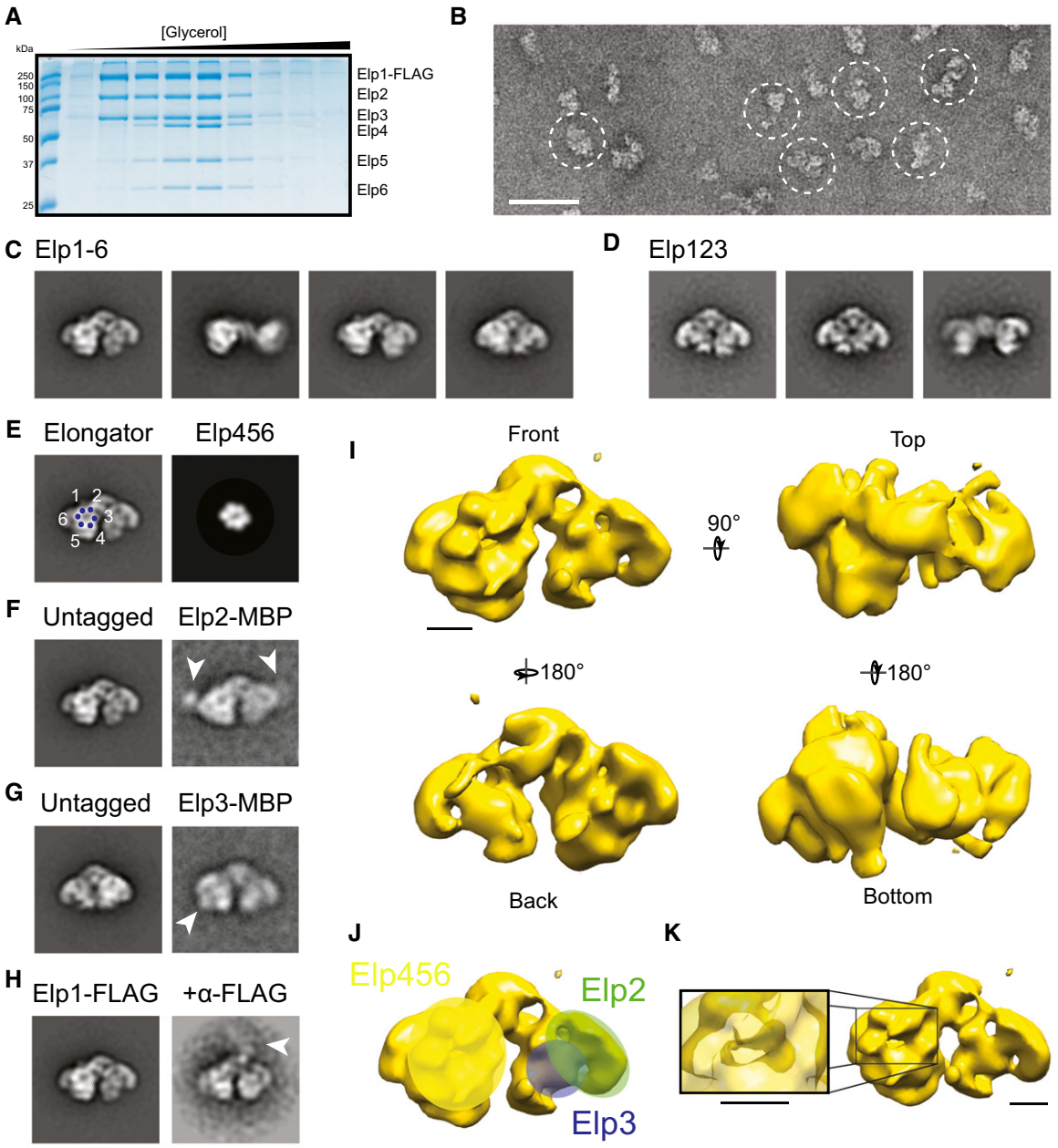

Figure 1. Elongator is a two-lobed asymmetric complex.

A Coomassie Blue-stained SDS–PAGE of yeast Elongator isolated by FLAG affinity purification and glycerol gradient ultracentrifugation from a strain encoding C-terminally FLAG-tagged Elp1.

B Representative segment of an electron micrograph of negatively stained Elongator after stabilization by gradient fixation (lane 6 of panel A). Circled particles correspond to intact Elongator. White scale bar corresponds to 50 nm.

C Representative 2D class averages of the full Elongator complex from a total of 17,074 particles.

D Representative 2D class averages of the Elp123 subcomplex prepared through a high salt dissociation procedure.

E Six evenly sized densities are arranged in one Elongator lobe. A projection of the Elp456 hexamer X-ray structure (PDB code: 4A8J) is shown for comparison.

F Analysis of Elp2 localization using a C-terminal MBP tag. Class averages of untagged Elongator are shown for comparison. White arrowheads point toward additional densities in the tagged complex.

G Elp3 localization analysis using a C-terminal MBP tag, denoted by the white arrowhead.

H Mapping of Elp1 by incubating purified Elongator containing an Elp1 C-terminal FLAG tag with α-FLAG antibody. The additional antibody density is denoted by the white arrowhead.

I Three-dimensional reconstruction of the intact Elongator complex at 25 Å.

J Schematic of the approximate subunit locations based on 2D EM analysis.

K Inset showing the cavity formed through the center of the putative Elp456 density.

Data information: All class averages shown in this figure have side width of 500 Å. Black scale bars in this figure correspond to 50 Å.

analysis showed that the peak fraction obtained from an identical gradient run without cross-linker contains stoichiometric quantities of each of the six Elongator subunits (Table EV1), confirming that this procedure preserved the integrity of Elongator. Negative stain EM analysis of purified Elongator showed elongated, bilobal particles with dimensions of approximately 300 Å × 200 Å (Fig 1B). Subsequent two-dimensional (2D) classification analysis revealed that Elongator adopts an overall shape resembling a moth, with two prominent triangular-shaped "wings" connected at two corners by a small central density (Fig 1C panel 1).

The Elongator subunits have been proposed to associate into a symmetric complex, with two Elp123 subcomplexes connected to one another via the hexameric ring assembly formed by Elp456 [15]. To our surprise, our 2D analysis showed that the majority of Elongator adopts an asymmetric architecture (Fig EV1A). In particular, the most populated 2D class averages of intact Elongator show particles with a ring-shaped density perched on top of one of the two wings. Interestingly, no particles containing two ring-shaped densities were observed in our dataset (Fig EV1A). In addition to the unique asymmetric architecture, our 2D analysis also revealed variability in the distance between the two lobes of the complex, with some particles showing a more "open" conformation (Fig 1C panel 3, and Fig 1D panel 1) and others a more "closed" conformation (Fig 1C panel 4, and Fig 1D panel 3).

The overall dimensions and hexameric shape of the ring-shaped density resemble that of the projection view of the Elp456 crystal structure (Fig 1E). To determine whether Elp456 constitutes this density, we isolated the Elp123 subcomplex from the Elp1-FLAG strain using a high salt purification strategy that dissociates Elp456 from the full Elongator complex [14]. Class averages obtained from 2D EM analysis of purified Elp123 show particles with both lobes lacking the ring-shaped density (Figs 1D and EV1B and C). This result not only confirmed that Elp456 indeed binds to only one half of the Elp123 dimer in the intact complex but also showed that two Elp123 subcomplexes can dimerize in the absence of Elp456.

We next took an EM-based labeling approach to further investigate the organization of Elp123. We isolated Elongator containing C-terminal maltose binding protein (MBP) tagged Elp2 or Elp3 and localized the MBP labels by negative stain EM. We found that Elongator containing either MBP-tagged Elp2 or Elp3 displays additional densities at either the furthest corners or the posterior edge of the Elongator "wings" (Fig 1F and G). Only one Elp3-MBP density could be resolved from our 2D analysis. We attribute this to the class averaging procedure aligning one copy of the tag, while the variable relative position of the second tag resulted in its density being averaged down to background levels. To map the location of Elp1 C-terminus, we applied a similar EM-based approach using antibody-based labeling (Fig 1H). We observed an additional density corresponding to the antibody attaching to the tube-like density connecting the two Elongator lobes, a location consistent with recent findings that the Elp1 C-terminal domain mediates complex dimerization [16]. Collectively, these results indicate that Elp2 and Elp3 are positioned along the distal corners and posterior edges of the moth-shaped complex, respectively, while the Elp1 C-terminus likely forms the bridge between the two lobes of Elongator.

The limited yield of our native complex purification has prevented us from preparing vitrified specimens and characterizing this complex at higher resolution by cryo-EM. We therefore determined a three-dimensional (3D) reconstruction of Elongator from our negative stained specimens (Figs 1I and EV2). The resulting ~25 Å resolution structure confirmed that one of the two wing-shaped lobes houses an additional density with size and shape resembling the Elp456 hexamer. The plane of the Elp456 hexamer is angled approximately 30 degrees away from the complex plane (Fig 1I, top view) with the posterior edge closest to the Elp123 core complex. Aside from the putative Elp456 hexamer, each lobe can be divided into three main densities arranged adjacent to each other. Based on our MBP-tagging experiments, we assigned the distal and central densities as Elp2 and Elp3, respectively (Fig 1J). Furthermore, the EM density map revealed a slender cavity, approximately 80 Å deep, that projects into the Elp123 lobe through the center of the Elp456 hexamer (Fig 1K).

Subunit connectivity of holo-Elongator

To gain further insights into the subunit connectivity of Elongator, we generated knockouts of three *elp* genes (*elp1*Δ, *elp2*Δ, or *elp3*Δ) in a FLAG-tagged Elp4 background strain, and performing mass spectrometry analysis of anti-FLAG affinity purified samples from these three yeast strains to determine the effects of these mutations on complex formation (Fig 2A). We found that Elp5 and Elp6 co-purified with Elp4 in all three mutants, suggesting that the Elp456 ring can assemble independently of Elp123. Our analysis also showed that Elp1 is essential to the binding of Elp2 and Elp3 to Elp456, while Elp2 deletion has no effects on the association of Elp1 and Elp3 to Elp456. Finally, Elp3 deletion severely disrupts Elp2 but not Elp1 binding to Elp4. Results from these studies are consistent with the observed peripheral location of Elp2 and in addition indicated that Elp1 not only mediates complex dimerization but also serves as the major scaffold for other Elongator subunits to assemble.

To gain molecular insights into subunit organization, we subjected purified Elongator to cross-linking coupled to mass spectrometry (CXMS) analysis. We incubated purified Elongator with the cross-linker disuccinimidyl suberate (DSS) (Fig EV3) and analyzed the cross-linked peptides by mass spectrometry to identify lysines in close proximity to each other (Fig 2B–D). We found that 24 out of 25 cross-linked residues observable in available high-resolution structures of Elongator subunits were within the 30 Å maximum Cα-Cα distance allowable by DSS [19] (Table EV2).

The Elp1 N-terminal domain, Elp2, Elp3, and Elp4 contained the highest number of cross-links, suggesting that these subunits likely form the primary interaction interface of the complex (Fig 2B–D). Elp3 was found cross-linked to every unique subunit of Elongator. This observation is consistent with the central location of this subunit deduced from our EM-based labeling analysis. Furthermore, by mapping the cross-linked residues onto the crystal structure of the core Elp456 hexamer [13], we found that the β-sheet-rich face of the Elp456 housing the N- and C-termini of Elp5 and Elp6 is likely oriented toward the Elp123 core complex.

Conserved loop regions of Elp2 are crucial to Elongator function

To further validate our CXMS data, we probed a series of four loop regions in Elp2 that were found to be cross-linked to other Elongator subunits. We hypothesized that these loops are important for Elp2's role in Elongator function, possibly in stabilizing major

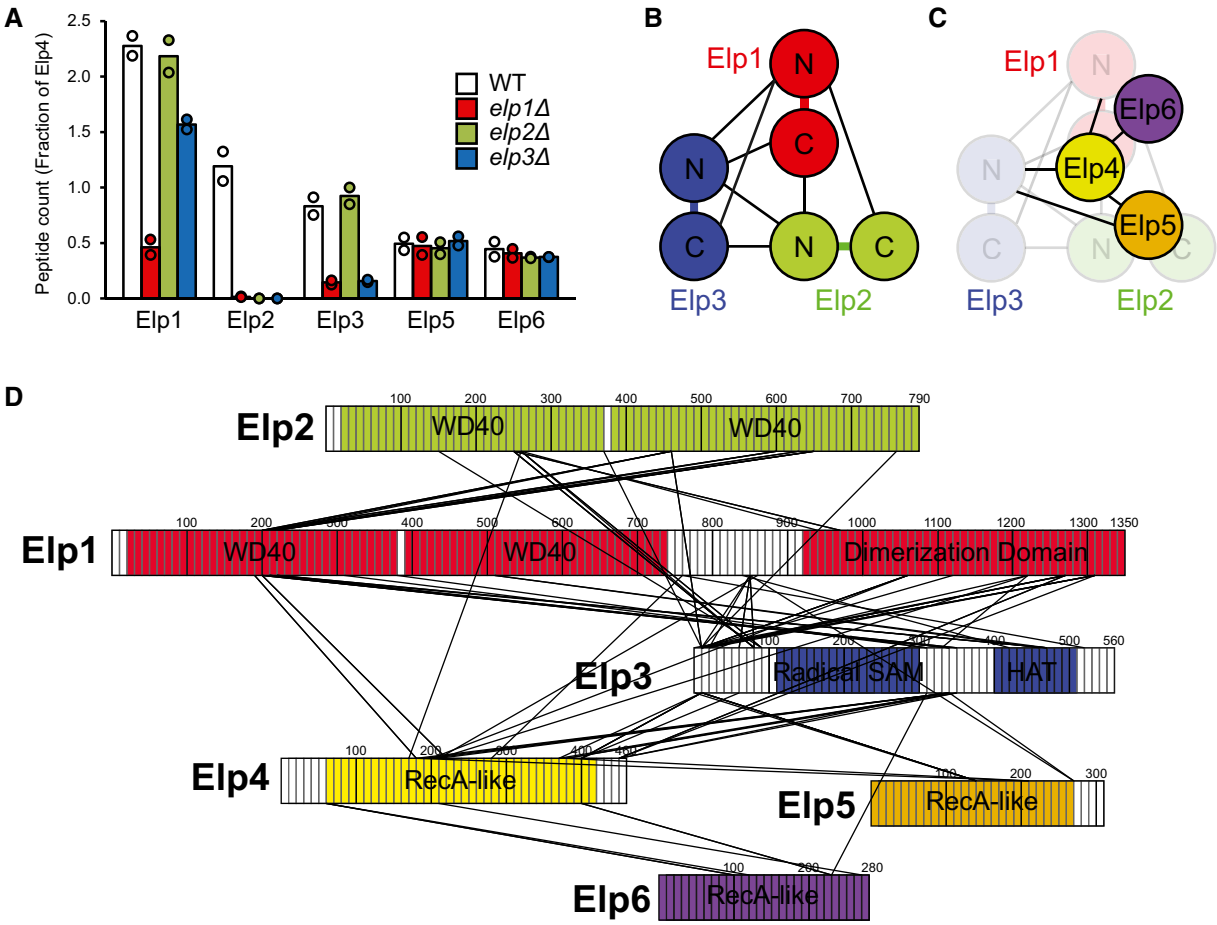

Figure 2. Mass spectrometry analysis of Elongator.

A Number of peptides detected of each Elongator subunit purified through Elp4-FLAG pull-down from yeast lacking ELP1, ELP2, or ELP3 as a fraction of the number of Elp4 peptides. Individual data points are represented as circles, while the averages are represented as bars.

B Purified Elongator was incubated with the primary amine cross-linker disuccinimidyl suberate (DSS) and analyzed by mass spectrometry. Schematic representation of the major cross-linking connectivity of Elp123 is shown.

C Major cross-linking connectivity of the Elp456 complex.

D Detailed locations of cross-linked residues plotted onto a domain representation of Elongator. Lysines from two residues found cross-linked together are denoted by black lines.

interaction interfaces. We introduced alanine mutations to the conserved residues within four loops (Fig 3A) and examined their effects on Elongator function. We found that mutations in loops 1, 3, and 4 of Elp2 cause impaired growth on plates containing caffeine (Fig 3B). These mutants are also resistant to the *Kluyveromyces lactis* toxin zymocin, which specifically cleaves tRNA harboring U34 (wobble position) modification (Fig 3C) [20]. Both these phenotypes are consistent with impaired Elongator function [12,21].

We next evaluated the association of these Elp2 mutants to other Elongator subunits. We purified Elongator from strains expressing the Elp2 loop mutants and Elp4-FLAG using anti-FLAG affinity chromatography and probed the eluted proteins by Western blot (Fig 3D). We found that the Elp2 loop 2 mutations did not affect co-purification with Elp4-FLAG. By contrast, the loop 1 mutation results in substantially reduced level of Elp2 co-purified with Elp4 (Fig 3D). The loop 3 and 4 mutations led to a mild reduction in co-purification, suggesting that these loops mediate Elp2 function aside from complex assembly. These results confirm that the highly cross-linked, conserved residues in the loop 1, loop 3, and loop 4 regions of Elp2 are critical for Elongator function.

Model of yeast Elongator architecture

To visualize the overall architecture of Elongator, we took a multi-scale modeling approach that involves integrating: (i) EM mapping data; (ii) the subunit cross-linking patterns; (iii) the available crystal structures of Elp1 C-terminal domain [16], Elp2 [17], and the core Elp456 hexamer [13]; and (iv) and homology models of the Elp1 N-terminal WD40 and the Elp3 HAT and radical SAM domains to derive a "best fit" multiscale model representing the approximate overall architecture of Elongator (Fig 4). The Elp1 N-terminal tandem WD40 domains fitted to two stacked disk-shaped density in the junction between the two Elongator lobes (Fig 4A). Fitting of

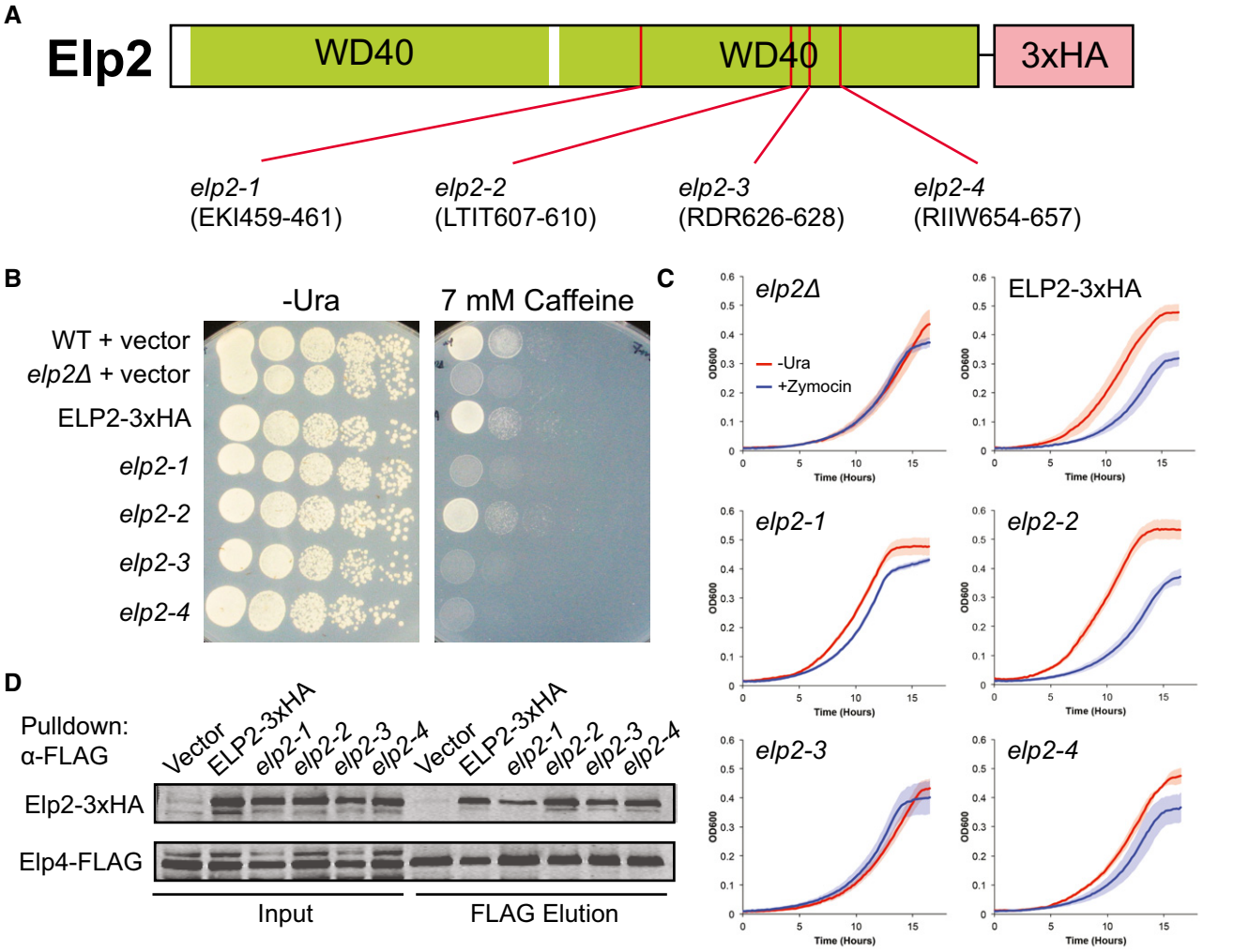

Figure 3. Conserved Elp2 loops are important for Elongator function.

A Schematic of the conserved residues within four Elp2 loops that were mutated to alanine within an ELP2 plasmid.

B Plasmids containing ELP2 and the four loop mutants were transformed into *elp2*Δ yeast. The strains were then plated onto –Ura media containing caffeine. The pRS416 vector was used for these experiments.

C Growth curve analysis of loop mutants in –Ura media with and without *K. lactis* toxin zymocin. Shaded regions correspond to the SEM at each time point. $N = 3$.

D Lysates of Elp4-FLAG-containing yeast expressing the Elp2 loop mutants were incubated with α-FLAG resin and eluted with 3xFLAG peptides and then analyzed by Western blot using α-HA and α-FLAG antibody

the Elp1 C-terminal dimerization domain, Elp2, and Elp3 was all consistent with the EM labeling experiments: Elp2 to the distal ends of the complex, Elp3 to the center of each lobe, and Elp1 C-terminus in the slender junction bridging the two lobes of the complex (Fig 4A). The X-ray structure of Elp456 fit unambiguously to the six-membered ring-shaped density consistent found in both 2D and 3D reconstructions of the intact complex (Fig 4B). The cavity through the center of the Elp456 ring is large and deep enough for a tRNA molecule to bind (Fig 4C).

Our model is consistent with our CXMS results, with direct access between cross-linked lysine pairs (Fig 4D). However, the distance between several Elp2-Elp1N cross-links exceeds the predicted DSS length. This is likely due to a combination of imperfect homology modeling of the Elp1 N-terminal WD40 domains and potential conformational flexibility of the Elp123 lobe. Flexibility within macromolecules often result in the violation of the allowable intersubunit cross-linking length [22,23], and movement within the Elp123 lobe may transiently shorten the distance between Elp1 and Elp2.

The resulting model shows that the two Elp1 subunits form a central scaffold and dimerize at their C-terminal regions, linking the two wing-shaped lobes. Elp1, Elp2, and Elp3 constitute the three adjoining densities forming the central framework of the complex. The lone Elp456 ring is anchored to one of the two Elp123 lobes. The 80 Å deep cavity spanning the center of Elp456 contacts the Elp3 HAT and radical SAM domains extensively (Fig 5B). Since residues lining the center of the hexamer were shown to be important for tRNA binding [13], and that this cavity can accommodate a tRNA molecule (Fig 5C), we speculate that this cavity might serve as the tRNA binding site.

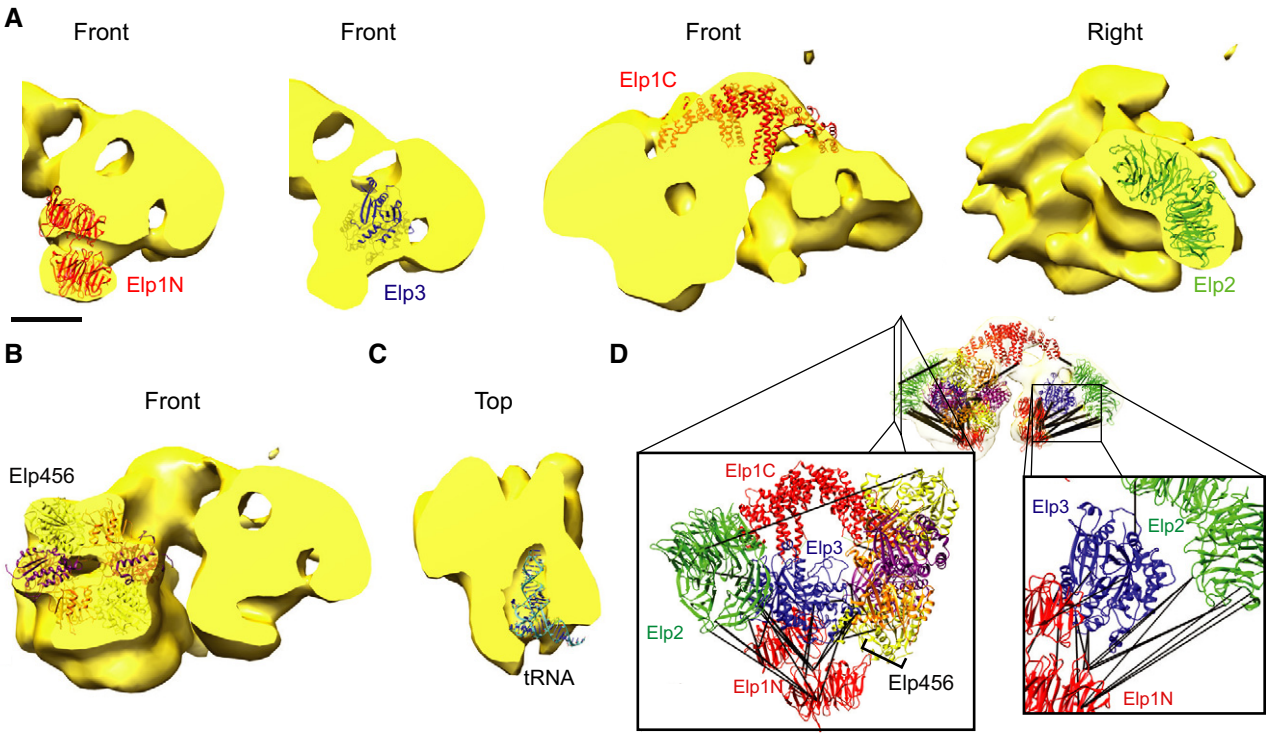

Figure 4. Fitting of Elongator subunits in the 3D reconstruction.

A Fitting of Elp123 structures into the 3D reconstruction of Elongator. The homology structure of the Elp1 N-terminal double WD40-domains, the homology structure of Elp3 based on the X-ray structure of *D. mccartyi* (5L7J), the X-ray structure of Elp1 C-terminal dimer (5CQS), and the X-ray structure of Elp2 (4XFV). Scale bar corresponds to 50 Å and applies to panels (A–C).

B Fitting of the Elp456 heterohexameric ATPase ring (4A8J) into the six-membered ring from the larger Elongator lobe.

C Size comparison of a representative tRNA molecule (1VTQ) and the cavity observed through the middle of the Elp456 hexamer.

D Alternate views of the Elongator model showing the subunit cross-linking patterns.

Our Elongator molecular model showed that the two Elp123 lobes are arranged in an asymmetric fashion. An implication of this finding is that Elp123 undergoes a conformational change upon binding of one Elp456 ring. To characterize this structural rearrangement further, we determined the three-dimensional reconstruction of the Elp123 subcomplex and then overlaid this structure into the EM density map of full Elongator (Figs 5C and EV4). Our analysis revealed that Elp123 adopts a more extended conformation (Figs 5C, front view, and EV4E) and a different rotational state relative to the putative Elp1 C-terminal bridge (Figs 5C, top view, and EV4F) compared to Elp123 within the full Elongator.

Elp123 can accommodate two of Elp456 hexamers

In addition to potentially enhancing interaction between Elp456 and Elp123, the observed conformational change of Elp123 might function to preclude the loading of a second Elp456 ring on the opposite Elp123 lobe. To test this hypothesis, we first need to verify that native Elongator contains only one Elp456 ring. Because Elp456 is sensitive to dissociation from the holo-complex in high salt conditions, we isolated Elongator from yeast cells using low salt buffer conditions (75 mM NaCl). Despite the presence of higher amount of contaminants in the purified complex, we were able to conduct 2D EM analysis on this "low salt" sample. The most populated class averages from this analysis show asymmetric, single Elp456-loaded particles that are indistinguishable from those obtained for Elongator purified using 150 mM NaCl (Figs 6A and B, and EV5A). However, to our surprise, we did detect a minor population of particles that contain prominent densities on both lobes (Fig 6B, class average indicated by a white triangle), suggesting that Elongator can accommodate two bound Elp456 rings.

To determine whether our purification procedure affects the Elp456 loading state of Elongator, we incubated native Elongator purified from yeast in buffer containing 150 mM NaCl with recombinant, catalytically active full-length Elp456 (rElp456) reconstituted in *Escherichia coli* (Figs 6C and EV5B and C) and subjected this mixture to glycerol gradient ultracentrifugation followed by Coomassie-stained SDS–PAGE and 2D EM analyses (Figs 6D–F and EV5D). As opposed to rElp456 which did not penetrate past the first three fractions of the same glycerol gradient (Fig 6D), a significant amount of externally supplied rElp456 co-migrated with the peak fractions corresponding to Elongator (Fig 6E). Densitometry analysis of the protein bands from the peak fraction revealed that there is approximately twice as much Elp4, Elp5, and Elp6 compared to Elp1 (Table EV3). Furthermore, the most populated class averages from 2D EM analysis of the peak fraction show particles with two

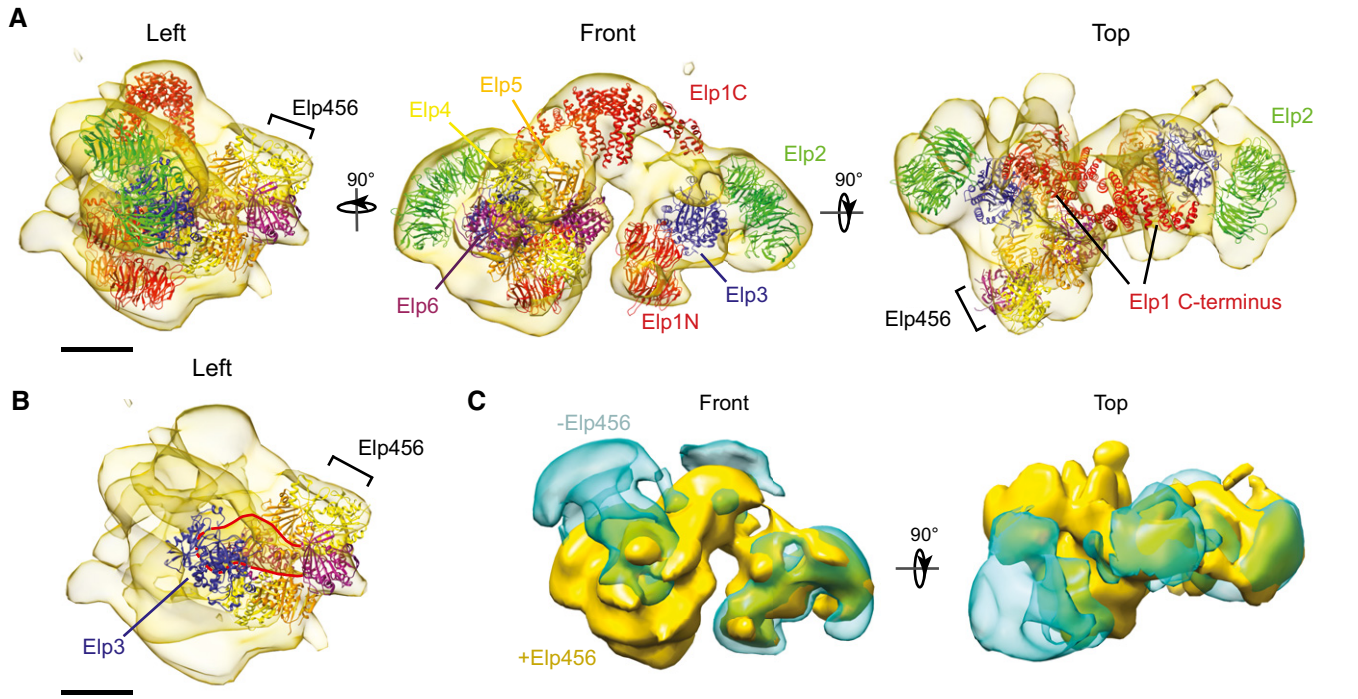

Figure 5. Model of Elongator subunit organization and Elp456 association.

A CXMS and EM data, combined with the X-ray structures of Elp1 C-terminus (5CQS), Elp2 (4XFV), Elp456 (4A8J), and homology models of the Elp1 tandem WD-40 domains and Elp3, were used to estimate the relative positions of each subunit to generate a multiscale model of Elongator subunit organization.

B Side view of the Elongator architectural model highlighting the cavity (red outline) spanning through the center of the Elp456 hexamer.

C Comparison of the Elp123 conformations of the intact Elongator complex (gold) and the Elp123 subcomplex (cyan). The Elp456-unloaded lobe of Elongator and one lobe of Elp123 were aligned.

hexameric ring-shaped densities decorating each of its two lobes (Figs 6F and EV5D). Collectively, these results confirm that the two copies of Elp456 subcomplexes can be stably anchored to Elongator even in moderate salt conditions we used in our purification procedure, and that the observed single-loaded nature of our purified native complex potentially results from limiting quantities of Elp456 in the yeast cytoplasm.

Discussion

This study presented the first comprehensive structural investigation of the intact Elongator complex. Previous studies have shown that Elongator is inherently dimeric and consists of two copies of six unique protein subunits [13]. Glatt *et al* proposed that Elp456 acts as a centrally located bridge between the two Elp123 subcomplexes. However, this model was challenged by the recent crystallographic analysis of the Elp1 C-terminal domain, which revealed that this domain self-dimerizes and facilitates Elongator dimerization [16]. Our results clearly show that the Elp456 heterohexamer is anchored to only one Elp123 lobe and distal to the dimerization interface. The 3D reconstruction of Elongator shows a long and slender bridging density, consistent with the alpha-helical repeats of the C-terminal TPR/IKAP dimerization domain [16]. Therefore, we conclude that Elongator is an asymmetric "dimer of multimers" likely connected by the Elp1 C-terminal region. These findings were validated by a similar negative stain EM- and CXMS-based study of yeast Elongator from the Müller group, who obtained an essentially identical structure and observed similar subunit arrangement [24]. We also observed that Elp123 changes conformation upon Elp456 binding (Fig 5C). Interestingly, the family of RecA-like ATPases that Elp456 belongs to contain many examples of molecular motors, such as helicases and transporters that utilize NTPs to conduct mechanical work [25]. The conformational changes of Elp123 could potentially be induced by Elp456's catalytic activity.

The mechanism limiting Elp456 association to only one Elp123 lobe is not known. We observed that the majority of front views of the complex contain only one copy of the Elp456 ring. A minor population of particles generated a class average with no discernable ring densities essentially identical to the class averages of the purified Elp123 subcomplex (Fig EV1A and C). Furthermore, none of the class averages we obtained for full Elongator show two Elp456 rings associated with both Elp123 lobes. However, we show that incubating purified Elongator with an excess of recombinant Elp456 subcomplexes results in the association of two heterohexameric rings to both Elp123 lobes (Fig 6F). This experiment indicates that there is no direct mechanism preventing double loading of Elp456 subcomplexes to Elp123. However, we also show that complexes purified from yeast, even under low salt conditions, mostly only contain one Elp456 ring (Fig 6B). Elongator stoichiometry may therefore be regulated at the level of expression to control to available pool of Elp456. Indeed, Elp1, Elp2, and Elp3 have been

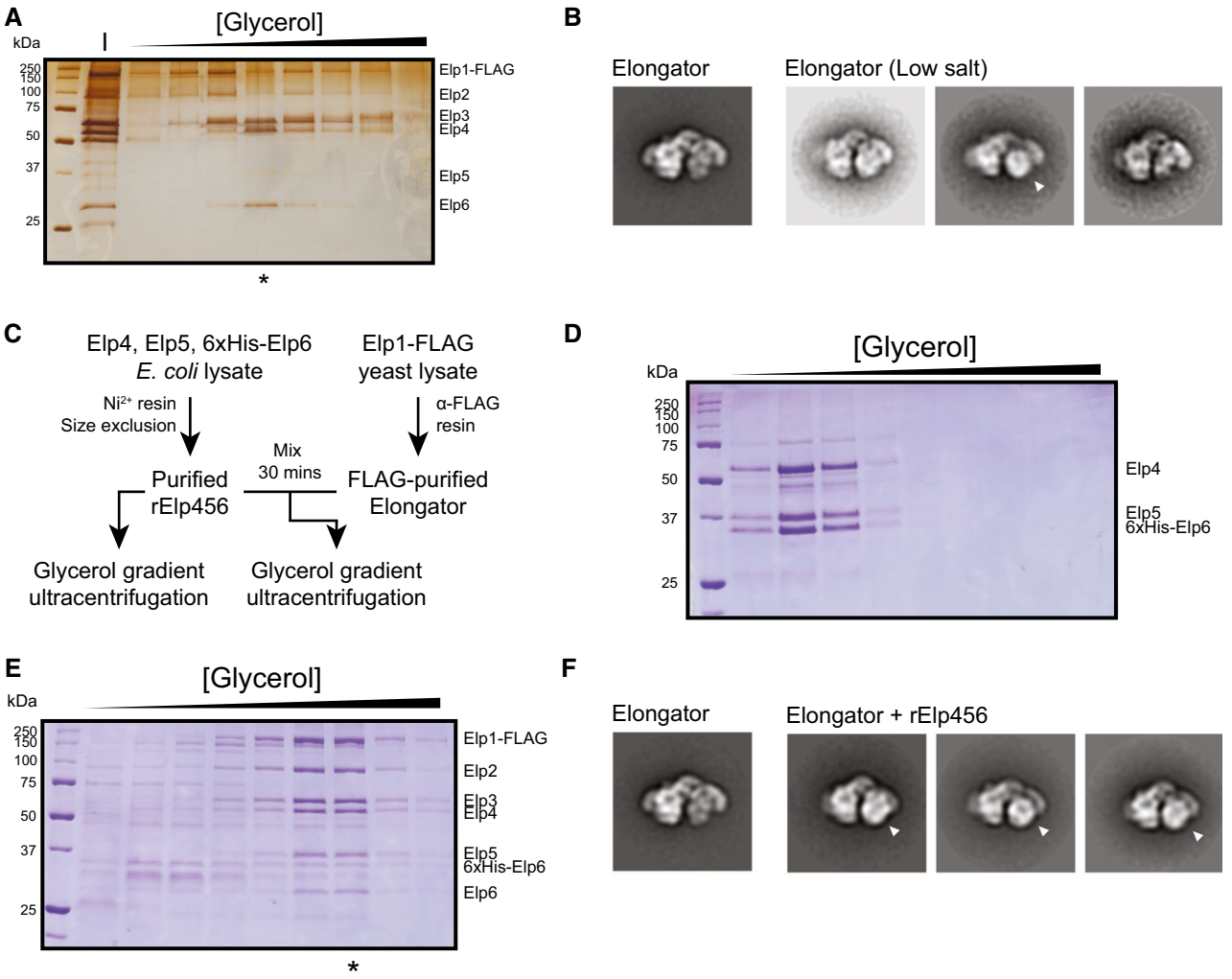

Figure 6. Elongator can accommodate two copies of the Elp456 subcomplex.

A Silver-stained SDS–PAGE of Elongator glycerol gradient fractions purified using low salt (75 mM NaCl) buffer. The fraction containing the most Elp4, Elp5, and Elp6 is designated by an asterisk (*) and the corresponding fraction from a glutaraldehyde-containing glycerol gradient is used for EM analysis.

B Comparison of class averages of Elongator purified in buffer containing regular or low salt concentrations (150 mM and 75 mM NaCl, respectively). Density resembling a second copy of Elp456 is indicated by a white triangle.

C Scheme of the Elongator and rElp456 mixing experiment. Recombinant Elp456 subcomplex (rElp456) was purified from *E. coli* and mixed with native yeast Elongator in regular salt conditions. The mixture, as well as rElp456 alone, was then subjected to glycerol gradient ultracentrifugation.

D Coomassie-stained SDS–PAGE of rElp456 glycerol gradient fractions.

E Coomassie-stained SDS–PAGE of the Elongator mixed with rElp456 glycerol gradient fractions. The fraction containing the most intact complexes is indicated with an asterisk (*), and the corresponding fraction from a glutaraldehyde-containing glycerol is used for EM analysis.

F Comparison of class averages of natively purified Elongator with and without rElp456 incubation. Densities resembling a second copy of Elp456 are indicated by white triangles.

shown to be more abundant in the cell than Elp4, Elp5, and Elp6 [26].

Our study provides the first insight into the structure of the holo-Elongator complex. In order to improve upon our architectural model, high-resolution structural data on the Elp1 N-terminal domain and Elp3 as well as the intact complex will be required. Whether Elongator contains two copies of the Elp456 hetero-hexamer *in vivo* remains an open question. We and others have shown that purified Elongator is most stable in conditions that result in a 1:1:1:1:1:1 subunit stoichiometry [12,13], but whether the 1:1:1:2:2:2 complex is present and functional *in vivo* still needs to be addressed in future studies.

Materials and Methods

Yeast methods and strain construction

Standard *S. cerevisiae* genetics and culturing methods were used. A list of strains and plasmids used in this study is provided in Table EV4.

Purification of yeast Elongator

To isolate the yeast holo-Elongator complex, 4 l of *S. cerevisiae* strains expressing C-terminally FLAG-tagged Elp1 was grown to an OD_{600} of ~4, harvested, and lysed by freeze grinding using a SPEX 6870 freezer mill (SPEX SamplePrep LLC, Metuchen, NJ). Freeze-ground yeast was resuspended in lysis buffer (40 mM HEPES pH 7.4, 150 mM NaCl, 10% glycerol, 1 mM EDTA, 1 mM PMSF, 50 mM NaF, 0.1 mM Na_3VO_4, 2 mM benzamidine, and cOmplete EDTA-free protease inhibitor [Roche]) and pre-cleared by ultracentrifugation at 154,000 × *g* for 30 min. Clarified lysate was incubated with 500 μl anti-FLAG M2 resin (Sigma-Aldrich, St. Louis, MO) at 4°C for 1 h. The resin was collected and washed three times with lysis buffer without inhibitors, incubated with 2.5 μg/ml RNase A for 30 min at 4°C, and washed 3× with lysis buffer without inhibitors. Bound Elongator was eluted with 2 × 500 μl of elution buffer (lysis buffer without inhibitors containing 500 μg/ml 3×FLAG peptide (GenScript, Piscataway, NJ). Further purity was achieved by subjecting the FLAG eluate to glycerol gradient ultracentrifugation. More specifically, 200 μl of eluate was overlaid onto a linear 15–30% glycerol gradient, ultracentrifuged at 76,000 × *g* using an SW 55 Ti rotor (Beckman Coulter, Brea, CA), and fractionated using the Gradient Station (BioComp, Fredericton, Canada). For the final 3D reconstruction of Elongator, we utilized the GraFix method to enhance stability of the purified complex, with a glutaraldehyde gradient of 0–0.05% added to the glycerol gradient [27]. The initial random conical tilt model was prepared using Elongator particles isolated by glycerol gradient ultracentrifugation without glutaraldehyde. Preparation of Elongator in low salt conditions utilizes an identical purification procedure, except all buffers used contain 75 mM NaCl as opposed to 150 mM.

Preparation of the Elp123 subcomplex utilizes an identical FLAG pull-down procedure to that of the intact complex using Elp1-FLAG yeast, except all buffers used contain 300 mM NaCl. The FLAG eluate was concentrated using a 100 kDa cutoff centrifugal filter unit (Merck Millipore, Billerica, MA) and further purified by size-exclusion chromatography using a Superose 6, 10/300 column (GE Healthcare, Little Chalfont, UK).

The purification of Elongator with subunit deletions utilized the same general procedure, except that for these experiments only 1 l of yeast was used and lysis was performed using a coffee grinder (Krups, Solingen, Germany). Furthermore, the FLAG eluates were directly used for mass spectrometry analysis.

Antibody labeling analysis

GraFix-purified Elongator containing an Elp1 C-terminal FLAG tag was incubated with 50 μg/ml α-FLAG M2 antibody (Sigma-Aldrich, St. Louis, MO) for 10 min at room temperature.

Electron microscopy

The peak glycerol gradient fractions containing Elongator were adsorbed to glow-discharged carbon-coated grids and stained with uranyl formate as described previously [28]. The EM specimens were examined using a Tecnai Spirit G2 (FEI, Hillsboro, OR) operated at an accelerating voltage of 120 kV. Micrographs were acquired at a nominal magnification of 49,000× with an FEI Eagle 4K charge-coupled device (CCD) camera at a defocus of 1–1.5 μm. For collecting tilt pair data for determining an initial 3D model, the same area of the grid was imaged at 60° tilt and untilted.

Image processing

To determine the 3D reconstruction of Elongator, we first obtained an initial model using the random conical tilt approach implemented in the SPIDER software suite [29]. In brief, tilt pair particles from the tilt pair dataset were selected using WEB, with the untilted particles subjected to alignment and classification. Tilted particles from the most populated classes were used to calculate a reconstruction using the back projection procedure.

For the final Elongator reconstruction, we collected 100 micrographs which were phase-flip CTF corrected using CTFFIND3 and SPIDER (final pixel size 7.0 Å/pixel) [29,30]. The micrographs were subjected to template-based autopicking in RELION to obtain a total of 17,074 particles [31]. These particles were then aligned and classified using maximum likelihood methods and the averages for each class calculated using RELION (Fig EV1). These class averages were used for the 2D analysis of intact Elongator. Bad particles were excluded to yield a particle count of 9,962. The particles were then subjected to RELION 3D classification using the RCT model as a reference. Classes of inferior quality were discarded for a final particle count of 8,190. The final set of particles were used to refine the most highly populated class from 3D classification using RELION's auto-refine feature. At no point did we discriminate between "open" and "closed" lobe conformations of the complex. After postprocessing without map sharpening, a final resolution of 25 Å was calculated at the 0.143 FSC criterion using the gold-standard method [32]. Details on this process can be found in Fig EV2.

Similar procedures were used for the Elp123 reconstruction. 28,121 particles were extracted from 106 phase-flipped micrographs. Bad particles were discarded after 2D alignment and classification, and 16,362 particles were used for 3D classification with the RCT reconstruction of intact Elongator as an initial model. All particles segregated to classes resembling Elongator and were used to refine the highest quality 3D model. As with full Elongator, we did not discriminate between the "open" and "closed" conformations of the complex.

For subunit localization 2D image analysis, all micrographs were binned twice to give a final pixel size of 4.67 Å/pixel. Individual particles were selected using EMAN Boxer [33]. Particle images were then aligned and classified in either SPIDER [29] or RELION to generate the class averages. No significant differences between the performances of these two software suites were detected. Particles from class averages showing additional C-terminal MBP tag density were subjected to a second round of alignment and classification to further segregate particles with the additional MBP density. The same procedure of classification and subclassification was employed to determine the location of the anti-FLAG antibody bound to Elongator containing Elp1-FLAG.

Cross-linking coupled to mass spectrometry

FLAG-purified Elongator (without glycerol gradient ultracentrifugation) was incubated with either 40, 80, 160, 240, 320, 480, or

640 μM of disuccinimidyl suberate (DSS) for 30 min at room temperature. This range of cross-linker concentrations was determined to generate both lightly and extensively cross-linked complexes by SDS–PAGE across two experiments with slightly different preparation methods until a satisfactory number of cross-linked peptides were detected. Reactions were quenched using 50 mM Tris–HCl pH 8.0 for 15 min at room temperature. Cross-linked samples were separated on 5–20% SDS–PAGE (Bio-Rad, Hercules, CA) followed by Coomassie Blue G-250 staining (Fig EV3). The high molecular weight band corresponding to the cross-linked complex was excised and subsequently processed for mass spectrometry analysis as previously described [34]. Both experimental samples were digested with a combination of 10 ng/μl trypsin and 5 ng/μl Lys-C. Digested products were analyzed on a Q Exactive MS instrument equipped with an Easy nano-LC 1000 liquid chromatography system (ThermoFisher Scientific, Waltham, MA). Digested peptides (~0.5 μg) were loaded onto 75 μm × 6 cm trap column that was packed with 10 μm, 120 Å ODS-AQ C18 resin (YMC, Kyoto, Japan) and connected through a microTee to a 75 μm × 10 cm analytical column packed with 1.8 μm, 120 Å UHPLC-XB-C18 resin (Welch Materials, Shanghai, China). Peptides were separated over a 100-min linear gradient from 100% buffer A (0.1% FA) to 30% buffer B (100% ACN, 0.1% FA) and then a 10-min gradient from 30% to 80% buffer B, reaching 100% buffer B in the next 1 min and maintaining at 100% buffer B for 2 min before returning to 100% buffer A in 3 min and ending with a 4-min 100% buffer A wash. The flow rate was 200 nl/min.

MS parameters: Top 20 most intense ions are selected for MS2 by HCD dissociation; R = 140,000 in full scan, R = 17,500 in HCD scan; AGC targets were 1e6 for the full scan, 5e4 for MS2; minimal signal threshold for MS2 = 4e4; +1, > +6 and unassigned precursors were excluded for identifying immune-precipitated products which +2 precursors were also excluded for cross-linking samples; normalized collision energy is 27 for HCD; and peptide match is preferred.

Identification of cross-linking peptides and interacting proteins

The MS data were analyzed using the pLink software tool [35] to identify cross-linked peptides. The pLink search parameters were as follows: The protein database consisted of the sequences of six Elongator subunits and the proteases used to digest samples; maximum number of missed cleavages (excluding the cross-linking site) = 3; min. peptide length = 4 amino acids; and cysteine carbamidomethylation was set as fixed modification. pLink search results were filtered by requiring FDR ≤ 0.05 and a mass deviation ≤ 10 ppm of the observed precursor from either the mono-, the first, second, third, or fourth isotope of the matched candidate. Then, the inter-linked peptides were further filtered by E-value < 0.0001 and spectra count ≥ 2.

Identification of co-purified proteins from Elongator subunit deletion strains

Proteins co-purified with Elp4-FLAG from either *elp1*Δ, *elp2*Δ, or *elp3*Δ mutant strains were identified by searching the MS data against a UniProt *S. cerevisiae* protein database using Prolucid [36]. The Prolucid search results were filtered using DTASelect 2 [37] by requiring ≤ 1% FDR at the peptide level. The protein FDR was < 6%. Technical duplicates were performed.

Yeast phenotypic assays

Single colonies of each strain were grown in 5 ml Ura– medium at 30°C overnight with continuous shaking. For the zymocin growth curve assay, the overnight cultures were used to inoculate wells in a 48-well plate to a total volume of 200 μl per well and an OD_{600} of 0.1 in technical triplicates. Conditions and strains in each well were randomized on the plate to account for non-uniform heating. Certain wells only contained Ura– media for background correction. +Zymocin media consist of 4:5 volume of Ura– media and 1:5 volume of concentrated filtrate isolated from a culture of *Kluyveromyces lactis* (NCYC 1368). The plates were incubated in the BioTek Synergy HTX microplate reader (BioTek, Winooski, VT) at 30°C with continuous orbital shaking for 16 h. OD_{600} readings were taken every 10 min. For yeast plate assays, the cultures were grown to an OD_{600} of ~0.5 and a fivefold serial dilution is performed. 5 μl of each dilution was spotted onto –Ura with and without 7 mM caffeine plates. Each plate was incubated for 2 days at 30°C before imaging. Three biological replicates were performed.

Elp2 loop mutant co-purification

Elongator was purified from yeast strains expressing both Elp2 loop mutants and Elp4-FLAG using the FLAG affinity purification procedure described above, with few adjustments. Quantities of reagents and buffers used were adjusted for a starting culture volume of approximately 200 ml. Prior to incubation with α-FLAG M2 resin, the total protein concentration of the lysates was measured by Quick Start Bradford Protein Assay (Bio-Rad, Hercules, CA) and standardized across all strains analyzed. Glycerol gradient ultracentrifugation was not performed. Instead, FLAG elutions were analyzed by Western blot using α-HA antibody (Applied Biological Materials, Richmond, BC) and α-FLAG M2 antibody (Sigma-Aldrich, St. Louis, MO).

Construction of the multiscale model of Elongator

The EM map of intact Elongator was used as the basis for fitting. X-ray structures of the Elp1 C-terminus, Elp2, and Elp456 were obtained from PDB (5CQS, 4XFV, and 4A8J, respectively [13,16,17]), the homology structure of the Elp1 tandem WD40 domains was generated using Phyre2 [38], while the homology structure of Elp3 was generated by SWISS-MODEL [39] based on the X-ray structure of *Dehalococcoides mccartyi* (5L7J) [40]. Initial manual rigid body fitting was performed in UCSF Chimera [41] guided by the EM labeling experiments. Results from cross-linking coupled to mass spectrometry were used to provide additional restraints for further optimization of fitting of high-resolution structures within the map.

Overexpression and purification of recombinant Elp456 subcomplexes

Full-length yeast ELP4 and ELP5 were cloned into the pQLinkN vector and ELP6 was cloned into the pQLinkH vector containing an N-terminal 6xHis tag. The vectors were combined to make the pQLink-ELP4-ELP5-6xHis-ELP6 using ligation-independent cloning methods [42]. The proteins were expressed in T7 Express

competent *E. coli* (NEB, Ipswich, MA) at 18°C for 20 h using 1 mM isopropyl β-D-1-thiogalactopyranoside (Gold BioTechnology, St. Louis, MO). *E. coli* pellets were harvested and sonicated in lysis buffer (50 mM Tris–HCl pH 7.4, 300 mM NaCl, 5% glycerol, 10 mM imidazole, 1 mM DTT, 1 mM PMSF). Lysates were cleared by centrifugation at 31,000 × *g* and incubated with nickel-NTA resin (Thermo Fisher Scientific, Waltham, MA) for 1 h at 4°C, then washed six times with wash buffer (50 mM Tris–HCl pH 7.4, 300 mM NaCl, 5% glycerol, 50 mM imidazole). Bound proteins were eluted with elution buffer (50 mM Tris–HCl pH 7.4, 300 mM NaCl, 5% glycerol, 250 mM imidazole). The eluted proteins were loaded onto a Superdex 200, 10/300 GL (GE Healthcare, Little Chalfont, UK) size-exclusion chromatography column. The final buffer contains 20 mM Tris–HCl pH 7.5, 150 mM NaCl, 5 mM DTT, and 1 mM $MgCl_2$.

Malachite green ATPase assay

Purified rElp456 was added to assay buffer (15 mM Tris–HCl pH 7.5, 100 mM NaCl, 1 mM $MgCl_2$) with or without 0.5 mM ATP and incubated at 30°C for 30 min. Malachite green solution (Sigma-Aldrich, St. Louis, MO) was then added to the reaction and the absorbance at 620 nm was determined using the BioTek Synergy HTX microplate reader (BioTek, Winooski, VT). Absorbance readings were compared to a standard curve to calculate concentrations of free inorganic phosphate in each reaction. All assay conditions were performed in triplicate.

Elongator and recombinant Elp456 mixing experiment

FLAG eluates prepared from Elp1-FLAG as described above were incubated for 30 min on ice with purified recombinant Elp456 (rElp456) at a volume ratio of 3:1. The mixture, as well as rElp456 alone, was subjected to GraFix analysis as described above with identical buffer conditions.

Accession codes

The final reconstruction for the intact Elongator complex and the Elp123 subcomplex was deposited into the EM Databank (entry number EMD-8239 and EMD-8291, respectively).

Expanded View for this article is available online.

Acknowledgements
RELION 3D reconstruction computation was enabled by support provided by the WestGrid (www.westgrid.ca) and Compute Canada – Calcul Canada (www.computecanada.ca) Hungabee cluster. Molecular graphics and analyses were performed with the UCSF Chimera package developed by the Resource for Biocomputing, Visualization, and Informatics at the University of California San Francisco. We thank Christoph Müller and Carsten Sachse for discussion on verifying the handiness of the 3D reconstruction. This work was supported by a Natural Sciences and Engineering Research Council of Canada (NSERC) Discovery Grant (RGPIN 418157-2012), a Michael Smith Foundation for Health Research Career Investigator Award, a Canadian Institutes of Health Research (CIHR) New Investigator Award, and an infrastructure grant from the Canadian Foundation for Innovation (CFI) to CY and a NSERC CGS fellowship to DS.

Author contributions
DTS was involved in conception and design, acquisition of data, analysis and interpretation of data, and drafting or revising the article; DTHC, JMH, CHYL, and JLT were involved in acquisition of data; SL and UD were involved in acquisition of data and analysis and interpretation of data; M-QD was involved in analysis and interpretation of data; and CKY was involved in conception and design, analysis and interpretation of data, and drafting or revising the article.

Conflict of interest
The authors declare that they have no conflict of interest.

References

1. Otero G, Fellows J, Li Y, de Bizemont T, Dirac AM, Gustafsson CM, Erdjument-Bromage H, Tempst P, Svejstrup JQ (1999) Elongator, a multisubunit component of a novel RNA polymerase II holoenzyme for transcriptional elongation. *Mol Cell* 3: 109 – 118
2. Wittschieben BØ, Otero G, de Bizemont T, Fellows J, Erdjument-Bromage H, Ohba R, Li Y, Allis CD, Tempst P, Svejstrup JQ (1999) A novel histone acetyltransferase is an integral subunit of elongating RNA polymerase II holoenzyme. *Mol Cell* 4: 123 – 128
3. Kim J-H, Lane WS, Reinberg D (2002) Human Elongator facilitates RNA polymerase II transcription through chromatin. *Proc Natl Acad Sci USA* 99: 1241 – 1246
4. Li Q, Fazly AM, Zhou H, Huang S, Zhang Z, Stillman B (2009) The elongator complex interacts with PCNA and modulates transcriptional silencing and sensitivity to DNA damage agents. *PLoS Genet* 5: e1000684
5. Winkler GS, Kristjuhan A, Erdjument-Bromage H, Tempst P, Svejstrup JQ (2002) Elongator is a histone H3 and H4 acetyltransferase important for normal histone acetylation levels *in vivo*. *Proc Natl Acad Sci* 99: 3517 – 3522
6. Huang B, Johansson MJO, Byström AS (2005) An early step in wobble uridine tRNA modification requires the Elongator complex. *RNA* 11: 424 – 436
7. Esberg A, Huang B, Johansson MJO, Byström AS (2006) Elevated levels of two tRNA species bypass the requirement for Elongator complex in transcription and exocytosis. *Mol Cell* 24: 139 – 148
8. Creppe C, Malinouskaya L, Volvert M-L, Gillard M, Close P, Malaise O, Laguesse S, Cornez I, Rahmouni S, Ormenese S *et al* (2009) Elongator controls the migration and differentiation of cortical neurons through acetylation of α-tubulin. *Cell* 136: 551 – 564
9. Okada Y, Yamagata K, Hong K, Wakayama T, Zhang Y (2010) A role for the elongator complex in zygotic paternal genome demethylation. *Nature* 463: 554 – 558
10. Anderson SL, Coli R, Daly IW, Kichula EA, Rork MJ, Volpi SA, Ekstein J, Rubin BY (2001) Familial dysautonomia is caused by mutations of the IKAP gene. *Am J Hum Genet* 68: 753 – 758
11. Simpson CL, Lemmens R, Miskiewicz K, Broom WJ, Hansen VK, van Vught PWJ, Landers JE, Sapp P, Van Den Bosch L, Knight J *et al* (2008) Variants of the elongator protein 3 (ELP3) gene are associated with motor neuron degeneration. *Hum Mol Genet* 18: 472 – 481
12. Krogan NJ, Greenblatt JF (2001) Characterization of a six-subunit holo-elongator complex required for the regulated expression of a group of genes in *Saccharomyces cerevisiae*. *Mol Cell Biol* 21: 8203 – 8212

13. Glatt S, Létoquart J, Faux C, Taylor NMI, Séraphin B, Müller CW (2012) The Elongator subcomplex Elp456 is a hexameric RecA-like ATPase. *Nat Struct Mol Biol* 19: 314 – 320
14. Winkler GS, Petrakis TG, Ethelberg S, Tokunaga M, Erdjument-Bromage H, Tempst P, Svejstrup JQ (2001) RNA polymerase II elongator holoenzyme is composed of two discrete subcomplexes. *J Biol Chem* 276: 32743 – 32749
15. Glatt S, Müller CW (2013) Structural insights into Elongator function. *Curr Opin Struct Biol* 23: 235 – 242
16. Xu H, Lin Z, Li F, Diao W, Dong C, Zhou H, Xie X, Wang Z, Shen Y, Long J (2015) Dimerization of elongator protein 1 is essential for Elongator complex assembly. *Proc Natl Acad Sci USA* 112: 10697 – 10702
17. Dong C, Lin Z, Diao W, Li D, Chu X, Wang Z, Zhou H, Xie Z, Shen Y, Long J (2015) The Elp2 subunit is essential for elongator complex assembly and functional regulation. *Structure* 23: 1078 – 1086
18. Lin Z, Zhao W, Diao W, Xie X, Wang Z, Zhang J, Shen Y, Long J (2012) Crystal structure of elongator subcomplex Elp4-6. *J Biol Chem* 287: 21501 – 21508
19. Merkley ED, Rysavy S, Kahraman A, Hafen RP, Daggett V, Adkins JN (2014) Distance restraints from crosslinking mass spectrometry: mining a molecular dynamics simulation database to evaluate lysine-lysine distances. *Protein Sci* 23: 747 – 759
20. Lu J, Huang B, Esberg A, Johansson MJO, Byström AS (2005) The Kluyveromyces lactis γ-toxin targets tRNA anticodons. *RNA* 11: 1648 – 1654
21. Frohloff F (2001) Saccharomyces cerevisiae Elongator mutations confer resistance to the Kluyveromyces lactis zymocin. *EMBO J* 20: 1993 – 2003
22. Robinson PJ, Trnka MJ, Pellarin R, Greenberg CH, Bushnell DA, Davis R, Burlingame AL, Sali A, Kornberg RD (2015) Molecular architecture of the yeast Mediator complex. *eLife* 4: e08719
23. Chen ZA, Jawhari A, Fischer L, Buchen C, Tahir S, Kamenski T, Rasmussen M, Lariviere L, Bukowski-Wills J-C, Nilges M *et al* (2010) Architecture of the RNA polymerase II–TFIIF complex revealed by cross-linking and mass spectrometry. *EMBO J* 29: 717 – 726
24. Dauden MI, Kosinski J, Kolaj-Robin O, Desfosses A, Ori A, Faux C, Hoffmann NA, Onuma OF, Breunig KD, Beck M *et al* (2016) Architecture of the yeast Elongator complex. *EMBO Rep* 18: 264 – 279
25. Ye J, Osborne AR, Groll M, Rapoport TA (2004) RecA-like motor ATPases—lessons from structures. *Biochim Biophys Acta* 1659: 1 – 18
26. Kulak NA, Pichler G, Paron I, Nagaraj N, Mann M (2014) Minimal, encapsulated proteomic-sample processing applied to copy-number estimation in eukaryotic cells. *Nat Methods* 11: 319 – 324
27. Kastner B, Fischer N, Golas MM, Sander B, Dube P, Boehringer D, Hartmuth K, Deckert J, Hauer F, Wolf E *et al* (2008) GraFix: sample preparation for single-particle electron cryomicroscopy. *Nat Methods* 5: 53 – 55
28. Ohi M, Li Y, Cheng Y, Walz T (2004) Negative staining and image classification — powerful tools in modern electron microscopy. *Biol Proced Online* 6: 23 – 34
29. Frank J, Radermacher M, Penczek P, Zhu J, Li Y, Ladjadj M, Leith A (1996) SPIDER and WEB: processing and visualization of images in 3D electron microscopy and related fields. *J Struct Biol* 116: 190 – 199
30. Mindell JA, Grigorieff N (2003) Accurate determination of local defocus and specimen tilt in electron microscopy. *J Struct Biol* 142: 334 – 347
31. Scheres SHW (2012) RELION: implementation of a bayesian approach to cryo-EM structure determination. *J Struct Biol* 180: 519 – 530
32. Henderson R, Sali A, Baker ML, Carragher B, Devkota B, Downing KH, Egelman EH, Feng Z, Frank J, Grigorieff N *et al* (2012) Outcome of the first electron microscopy validation task force meeting. *Structure* 20: 205 – 214
33. Ludtke SJ, Baldwin PR, Chiu W (1999) EMAN: semiautomated software for high-resolution single-particle reconstructions. *J Struct Biol* 128: 82 – 97
34. Coffman K, Yang B, Lu J, Tetlow AL, Pelliccio E, Lu S, Guo D-C, Tang C, Dong M-Q, Tamanoi F (2014) Characterization of the raptor/4E-BP1 interaction by chemical cross-linking coupled with mass spectrometry analysis. *J Biol Chem* 289: 4723 – 4734
35. Yang B, Wu Y-J, Zhu M, Fan S-B, Lin J, Zhang K, Li S, Chi H, Li Y-X, Chen H-F *et al* (2012) Identification of cross-linked peptides from complex samples. *Nat Methods* 9: 904 – 906
36. Xu T, Park SK, Venable JD, Wohlschlegel JA, Diedrich JK, Cociorva D, Lu B, Liao L, Hewel J, Han X *et al* (2015) ProLuCID: an improved SEQUEST-like algorithm with enhanced sensitivity and specificity. *J Proteomics* 129: 16 – 24
37. Tabb DL, McDonald WH, Yates JR (2002) DTASelect and contrast: tools for assembling and comparing protein identifications from shotgun proteomics. *J Proteome Res* 1: 21 – 26
38. Kelley LA, Mezulis S, Yates CM, Wass MN, Sternberg MJE (2015) The Phyre2 web portal for protein modeling, prediction and analysis. *Nat Protoc* 10: 845 – 858
39. Biasini M, Bienert S, Waterhouse A, Arnold K, Studer G, Schmidt T, Kiefer F, Cassarino TG, Bertoni M, Bordoli L *et al* (2014) SWISS-MODEL: modelling protein tertiary and quaternary structure using evolutionary information. *Nucleic Acids Res* 42: W252 – W258
40. Glatt S, Zabel R, Kolaj-Robin O, Onuma OF, Baudin F, Graziadei A, Taverniti V, Lin T-Y, Baymann F, Séraphin B *et al* (2016) Structural basis for tRNA modification by Elp3 from Dehalococcoides mccartyi. *Nat Struct Mol Biol* 23: 794 – 802
41. Pettersen EF, Goddard TD, Huang CC, Couch GS, Greenblatt DM, Meng EC, Ferrin TE (2004) UCSF Chimera–a visualization system for exploratory research and analysis. *J Comput Chem* 25: 1605 – 1612
42. Scheich C, Kümmel D, Soumailakakis D, Heinemann U, Büssow K (2007) Vectors for co-expression of an unrestricted number of proteins. *Nucleic Acids Res* 35: e43